

Aleksandr WALISZYN
Andrzej ADAMKIEWICZ

STUDIES ON RESISTANCE TO EROSION OF NICKEL AND ITS ALLOYS TO BE USED IN ELEMENTS OF FLUID - FLOW MACHINES

BADANIA ODPORNOŚCI EROZYJNEJ NIKLU I JEGO STOPU DO ZASTOSOWANIA W ELEMENTACH MASZYN PRZEPEŁYWOWYCH*

The article presents results of studies on metal resistance to erosive damage taking place under the influence of hydraulic cavitation. On the basis of earlier research, a hypothesis on fatigue character of erosive wear and a dependence of metal resistance to erosive damage on its crystalline lattice structure has been assumed. To verify this hypothesis, metals with different crystalline lattice structures like steel 45 (flat-centred structure), nickel 200/201 and nickel alloy Monel 400 (hexagonal structure) have been tested at a cavitation-strike stand. Results obtained there confirmed the assumed hypothesis, at the same time justifying the use of nickel protective coatings in fluid-flow machines.

Keywords: physics of erosive contamination, resistance, operation, fluid-flow machine, nickel, nickel alloy.

W artykule przedstawiono wyniki badań odporności metali na uszkodzenia erozyjne zachodzące pod wpływem kawitacji hydraulicznej. Na podstawie wyników wcześniejszych badań, przyjęto hipotezę o zmęczeniowym charakterze zużycia erozyjnego oraz zależności odporności metali na zniszczenia erozyjne od struktury ich sieci krystalicznej. Dla potwierdzenia przyjętej hipotezy na stanowisku kawitacyjno-udarowym sprawdzono metale z różnymi sieciami krystalicznymi: stal 45 (sieć płasko centralna), nikiel 200/201 oraz stop niklu Monel 400 (sieć heksagonalna). Otrzymane wyniki badań potwierdziły przyjętą hipotezę, wskazując tym samym na zasadność stosowania niklowych powłok ochronnych w maszynach przepływowych.

Słowa kluczowe: zniszczenia erozyjne, odporność, maszyna przepływowa, nikiel, stopy niklu.

1. Physics of cavitation erosion in the cooling systems of diesel engines

Cavitation-erosive damage to fluid-flow machine surfaces washed by fluids and to heat exchange surfaces cooled by fluids is responsible for deterioration of the surface technical condition and decreases their durability. The cause of erosion is usually fluid cavitation in the machine working area. Despite a significant number of studies on cavitation origins of erosive damage to metal surfaces, the physics of fluid flux interaction with the surfaces of protective coating, especially damping ones remains an open case [3, 4, 7].

At present the theory of corrosive – erosive damage to cylinder liners of diesel engines has been widely acclaimed [1, 2]. Practically all researchers believe that the pre-cause of damage to the cooled surfaces of liners and cylinder blocks is the turbulent interaction of liquid with the metal surface being the result of cavitation bubble implosion. Erosive damage to liners and cylinder blocks, which is manifested by creation of clusters of deep cavities, is the result of complex interaction of mechanical and electrochemical processes damaging metal elements i.e. cavitation erosion and electrochemical corrosion. As a result of piston strike when the connecting-rod passes through upper and lower dead centres, cylinder liner experiences vibrations of high frequency which lead to changes in the speed of cooling liquid fluxes on the surfaces of liners and cylinder blocks [1, 13].

Local depressions and increases of liquid pressure which take place at the same time favour severing the continuity of the fluxes and creation of cavitation bubbles in the regions with lowered pressure. The bubbles are filled with vapour, gas or their two-phase mixture.

The change of pressure at any point of the liner surface washed by liquid may be evaluated with a dimensionless coefficient of local discharge [2]:

$$\xi = \left(\frac{v_0}{v_i} \right)^2 - 1, \quad (1)$$

where:

v_0 – mean speed of the liquid washing the surface of the liner,

v_i – flux speed in a chosen point i on the surface of the liner.

The largest depression p_i will be in the place where the value of ξ coefficient is maximal:

$$p_i = p_0 - q\xi, \quad (2)$$

where:

p_0 – mean pressure of the liquid,

q – pressure increase speed of the liquid flux:

$$q = \rho v_i^2 / 2, \quad (3)$$

ρ – liquid density.

The process of cavitation will start when p_i reaches the value equal to the pressure of saturated vapour p_n , at the environment temperature. Generation of cavitation bubbles takes place in the flux washing the surfaces of cylinder liners in the areas where the liquid flows through neckings and has the highest speed, whereas their implosion takes place in the lower speed range where the flux encounters flow

(*) Tekst artykułu w polskiej wersji językowej dostępny w elektronicznym wydaniu kwartalnika na stronie www.ein.org.pl

resistance or passes through spaces with widening cross-sections. The speed of water flow in cooling systems of diesel ship engines generally does not exceed 2 m/s and does not create conditions favouring hydrodynamic cavitation. Therefore, the basic cause of severing flux continuity should be ascribed to high frequency cylinder liner vibrations [14]. Their presence favours creating cavitation conditions in cooling water systems. Theoretical explanation of this is justified by the fact that when the dynamic pressure ($q = \rho g_i^2 / 2$) increases, the static pressure of the liquid decreases and conditions favouring flux severing are created. Stretching interactions of the cylinder liner being the result of vibrations add up to this.

Liquid possesses volume strength and to stretching stress. At the moment of equilibrium or exceeding volume strength under the influence of cylinder liner stretching stress, cavitation processes are initiated – vapour-gas bubbles are being formed. Bubble pulsation frequency is then equal to cylinder liner vibrations.

During the vapour-gas bubble implosion, liquid fluxes of very high speed (up to 34 m/s) appear on its surface, and the pressure of the liquid on the boundary of the imploding bubble and metal surface washed by water may exceed ($5 \cdot 10^6$) Pa. Then the striking energy of the cumulative flux particles is equal to:

$$E = fm\vartheta_k^2 \left[\frac{\eta_1 \omega}{6kT} + \frac{\eta_2}{c^2 \rho} \right]^{-1} \quad (4)$$

where:

- m – mass of the liquid of the striking flux,
- ϑ – cumulative flux speed,
- η_1, η_2 – kinematic viscosity coefficients of the liquid before and after the bubble implosion,
- ω – coefficient of internal friction of liquid molecules,
- K – Boltzmann’s constant,
- T – temperature,
- c – sound speed,
- f – coefficient accounting for events taking place until the bubble strikes.

The strike of the cumulative liquid flux onto the surface of a washed metal element leads to its plastic deformation and the increase of its hardness – work-hardening. Microcracks being the result of fatigue appear in the strengthened surface metal layers under further striking of cumulative liquid fluxes [8]. Their subsequent development leads to the formation of erosive pits in the form of craters. Figure 1 shows a diagram of metal damage caused by cumulative flux [2].

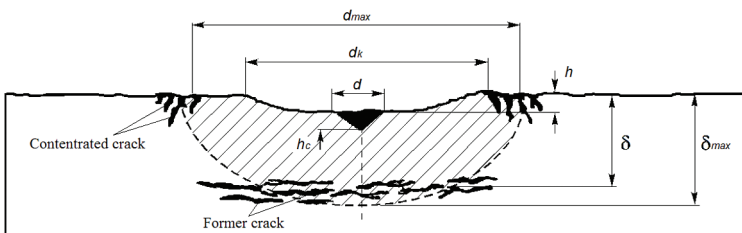


Fig. 1. A diagram of metal damage resulting from erosion cavitation d_{max} – maximum diameter corresponding to the area of concentrated cracks, d_k – pit diameter, d – diameter of oxidation product occurrence area, δ – depth of metal damage

Damage to metal takes place after reaching critical values of stress, which is characteristic for fatigue damage of materials. Frequently, in order to prevent erosive damage, technical literature suggests not very effective methods of increasing the hardness of the surfaces undergoing cavitation erosion. However, in the study [2] cavitation erosion intensity was defined by:

$$J = const \cdot H^n \quad (5)$$

where:

- J – erosive wear intensity (mg/mm²hour) of the metal;
- H – metal surface hardness (HB);
- n – exponent with values ranging from 2,78 (for carbon steels) to 0 (for chromium alloy steels).

The influence of initial steel hardness on the intensity of cavitation erosion is shown in Fig. 2 [12, 13]. Erosive damage to alloy steel 03HG10-10 with lower hardness in comparison to those used in the experiment was much smaller. Thus, in order to increase cavitation erosion resistance, the surface has to be more plastic.

The increase of resistance to cavitation erosion of metal surfaces can be reached throughout:

- making the working flux more laminar;
- covering metal surfaces with protective coatings
- damping vibrations of the element in the case of vibration cavitation.

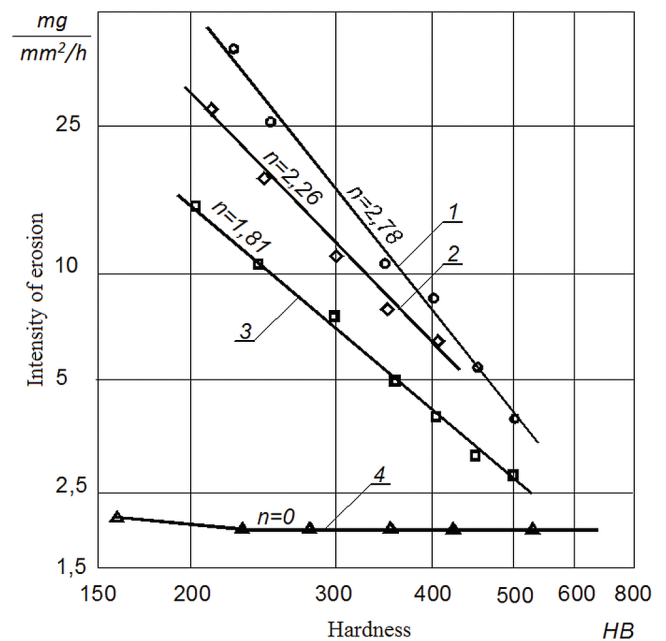


Fig. 2. Intensity of cavitation erosion in relation to initial steel hardness 1 – S40 i S1Cr40; Cr5V3; 2 – 1Cr13, 2Cr13, Mn20Si1; 3 – 1Cr18Ni3Mn4Cu2; 4 – 30Cr10Mn10

Laminar flow of liquid fluxes is connected with organising hydraulic systems in which liquid flux speeds do not exceed critical values corresponding with limiting values of the Reynold’s criterion. The critical value, marking the beginning of cavitation, is defined by a mathematical relation in the form of (6) [2]:

$$K_k = \frac{K_k^0}{C_j^0} (C_j - \Delta C_j^*) \quad (6)$$

where: K_k^0, C_j^0 – cavitation number and resistance coefficient of the by-wall non-laminar layer of the liquid flux:

ΔC_j^* – depending on the structure of the liquid flux, it is defined by:

$$\Delta C_j^* = \frac{1,33 \left(1 - \frac{1}{e^F} \right)}{\sqrt{R}} \quad (7)$$

where: e^F – limiting plasticity of metal surface washed by the liquid [2].

An analysis of equations (6-7) for the C_j^* resistance coefficient indicates that when the criterial Reynold's number decreases and when the plasticity of the washed surface increases, the resistance of the outer layer increases. Respectively, cavitation number K_k , which characterises conditions for cavitation phenomena initiation and damage connected with them, decreases.

Taking into account that at the initial moment, work hardening appears in the metal surface layer as a result of the influence of cumulative fluxes which in cyclic strike conditions gets damaged and cracks. Generated microcracks are the seeds of deep pits at then occurring crevice electrochemical corrosion. As a consequence erosive-corrosive damage can be treated as a fatigue-corrosive process. At the same time it can be stated that metal resistance to erosive-corrosive damage to a significant extent depends on the properties of the metal, its chemical composition and the properties of the surrounding medium.

Considering the fatigue character of erosive metal damage which takes place as a result of strikes of the liquid flux at the moment of explosions of vapour-gas cavitation bubbles, the following conclusions can be drawn. Strengthening of the metal surface layer and the resulting work-hardening as can be seen in Figure 1 is the initial stage of erosive damage. In the further development of the process, as a result of appearing fatigue stress, the strengthened metal surface gets cracked and later erosive cavities appear when simultaneously fatigue stress and crevice corrosion occur. Basing on the above conclusions, the most effective method preventing erosive damage to metal surfaces is to be found in the rational choice of mechanical properties of metals used in hydraulic installations. Obviously, the main condition of their application should be their inability to form strengthened surface layers which means that they should possess high plasticity.

2. Choice of study object

Considering maintenance of elasticity of single crystals of structural metals, one should take into account the anisotropy of elastic crystalline modules with the view to determining the differences in elastic deformation when the load is placed at different crystallographic directions. Most metals crystallise in three types of lattice: body-centred, face-centred or hexagonal lattice. These lattices are shown in Figure 3. In all of them, crystal face indexes are marked in the following way: along the X axis as [100]; Y axis - [010] and Z axis - [001]. Indexes of face diagonals are marked as [110] on the X-Y plane, [011] on the Y-Z plane and [101] on the X-Z plane; the body diagonal as [111]. Cast iron, steel and copper belong to metals with the face-centred lattice; nickel, zinc, aluminium and cadmium have hexagonal lattice. An important characteristics of metals from the point of view of their erosive resistance is their plasticity, which is shown in formula (7). Study [2, 3] notes that plasticity of metals with hexagonal lattice is higher than those with face-centred lattice. Deformation of these metals appears as a slide along the [001] plane, which does not lead to strengthening of the surface layer, that is to work-hardening. Deformation

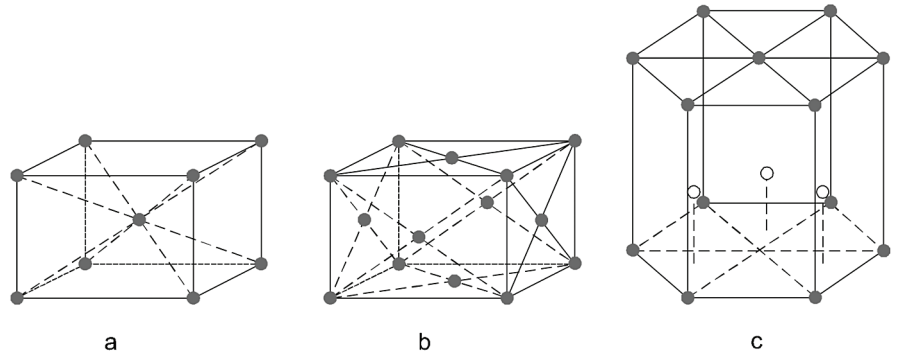


Fig. 3. Elementary cells of close packed lattices: a – body centred lattice; b – face-centred lattice; c – hexagonal lattice

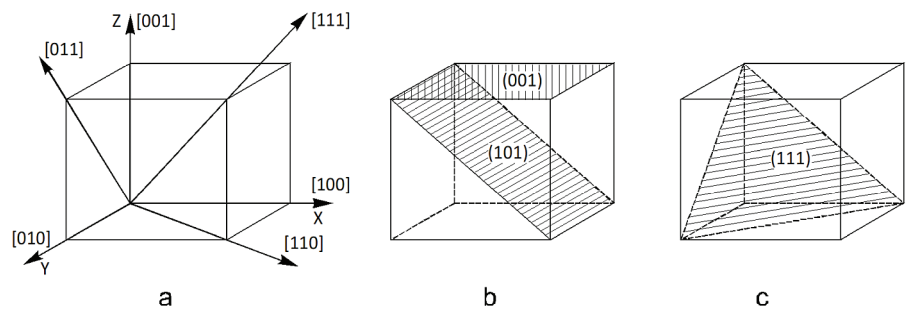
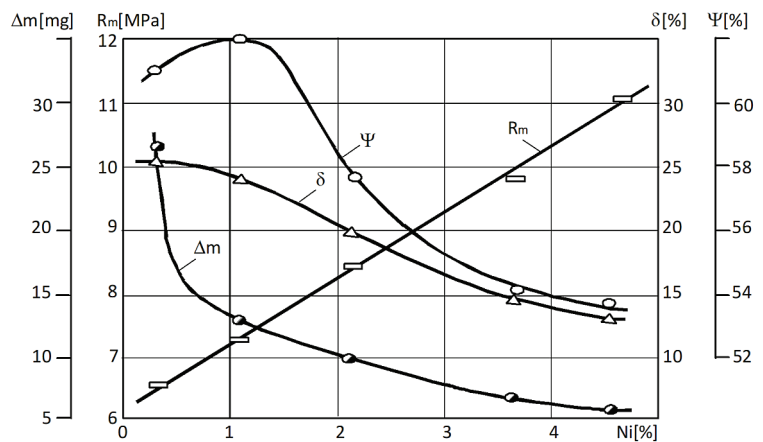


Fig. 4. Crystallographic indexes of deformation directions (a) and shear planes (b, c)

of metals with face-centred lattice in [111] and [112] planes is shown in Figure 4.

3. Comparative studies on resistance of metals with different crystalline lattice structure and their results

On the basis of an analysis of methods applied for studying metal resistance to cavitation erosive damage [14, 15], the method of ventilated cavitation has been chosen. As cavitation erosion is the effect of crashes of micro-fluxes of liquid after vapour-gas bubbles implosion, the experiment was carried out at a vibration stand using tap water as the working medium.



Δm – mass loss; R_m – temporary resistance; δ – relative elongation; Ψ – relative narrowing

Fig. 5. The influence of nickel content on the properties of alloy steels

Table 1. Chemical composition of samples with nickel 200/201

	C	Si	Mn	S	Co	Cu	Fe	Mg	Ti	Ni	Ni-Co
	0.01	0.04	0.10	<0.01	<0.01	<0.01	<0.01	0.102	0.04	99.67	99.687
Max	0.02	0.15	0.35	0.005	1.0	0.15	0.25	0.15	0.10		
Min											99.6

Table 2. Chemical composition of samples out of monel 400

	C	Si	Mn	Sr	Al	Co	Cu	Fe	Mg	Ti	Ni	Ni-Co
	0.13	0.23	0.94	0.03	<0.01	0.04	32.6	2.06		0.02	63.9	64.007
Max	0.15	0.5	2.0	0.02	0.5	1.0	34.0	2.5		0.3		
Min							28.0	1.0			36.0	63.0

Table 3. Results of studies of metal samples at a vibration stand

Mass (g)	Nickel			Monel			Steel C45		
	Sample 1	Sample 2	Sample 3	Sample 1	Sample 2	Sample 3	Sample 1	Sample 2	Sample 3
Mass for studies	9.0722	9.1200	8.8327	8.3740	9.7898	9.4627	8.7153	7.9301	7.8240
Mass after 10-min. exposition	9.0722	9.1200	8.8327	8.3739	9.7897	9.4626	8.7150	7.9298	7.8238
Mass after 30-min. exposition	9.072	9.1200	8.8327	8.3738	9.7896	9.4624	8.7147	7.9296	7.8235
Mass after 60-min. exposition	9.0717	9.1199	8.8325	8.3736	9.7894	9.4623	8.7140	7.9292	7.8231
Hardness of samples for studies (Vickers' method)	95.8	98.3	112.3	125.0	123.4	125.5	155.6	138.5	126.0
Mass decrease of samples during studies	0.0005	0.0001	0.0002	0.0004	0.0003	0.0013	0.0013	0.0009	0.0009
Mean metal decrease	0.00027			0.0007			0.001		
Speed of wear after a 10-min exposition (g/hour)	0			0.0018			0.0016		
Speed of wear after a 30-min exposition (g/hour)	0			0.0014			0.00106		
Speed of wear after a 60-min exposition (g/hour)	0.00027			0.0007			0.001		

Verification of the hypothesis of the fatigue character of erosive damage has been carried out for samples of three metals with different crystalline lattice structure: nickel 200/201, nickel alloy – monel 400 and constructional steel C45 [5, 6, 7]. Chemical composition of the studied nickel 200/201 and monel 400 samples is given in Tables 1 and 2.

Surfaces of samples of studied metals were polished to the roughness of 0,63 μm, after which the hardness of their upper layers was determined applying Vickers' method according to the PN-EN ISO 6507-1:2000 standard. The results, calculated as means of six measurements, are shown in Table 3.

Studies were carried out in compliance with the ASTM G32 standard in the option with an immobile sample in three series: with a 10-minute flux interaction on the sample, 30-minute and 60-minute long interactions. After each series, the samples were weighed using an analytical balance. Measurements of mass decrease enabled determination of the speed of erosive wear of the metals used in the experiment. Results of the studies are listed in Table 3 and graphically presented in Fig 6.

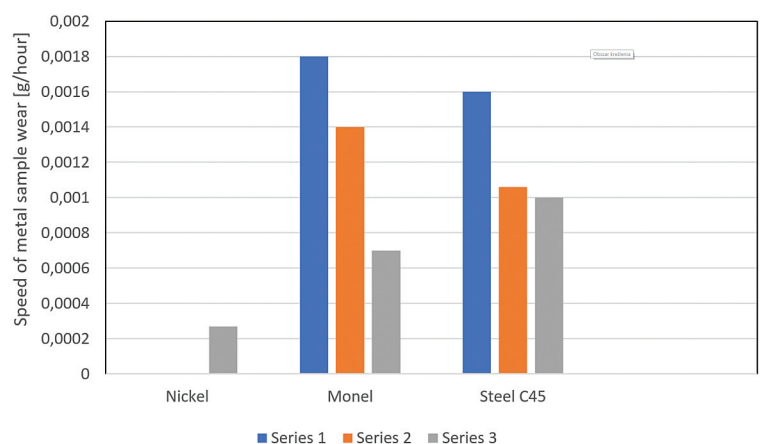


Fig. 6. Speed of erosive wear of metals in the experiment, where series 1 refers to a 10 minute long exposition, series 2 – 30 minute long and series 3 – 60 minute long exposition

4. Summary

Comparing the results of studies, it can be seen that Steel C45 has the lowest resistance to erosive wear in which case the speed of wear is thirty-seven times higher than that of nickel. Monel 400 reaches the values in-between. This fact also supports the assumed hypothesis of effectiveness of using plastic metals to prevent erosive damage in water installations which are prone to cavitation. The second fact supporting this hypothesis is the decrease of steel C45 and monel 400

wear with the increase of experiment time (Fig 6). It is the result of the increase of hardness of the sample upper layers and formation of work-hardening.

Summing up the carried out research, it can be said that prevention and slowing down erosive wear of working surfaces of fluid-flow machine parts may be achieved by using plastic metals to manufacture them.

References

1. Adamkiewicz A, Waliszyn A. Discussion and studies of the properties of a cooling water additive preventing erosive wear of cooled surfaces of ship diesel engines. *Eksploracja i Niezawodność - Maintenance and Reliability* 2014; 10(1): 565-570.
2. Adamkiewicz A, Waliszyn A. Studies of erosion resistance of protective coats on the surfaces of machine elements washed with fluids. *Advances in Materials Science* 2018; 6: 69-76, <https://doi.org/10.1515/adms-2017-0033>.
3. Amann T, Waidele M, Kailer A. Analysis of mechanical and chemical mechanisms on cavitation erosion/corrosion of steels in salt water using electrochemical methods. *Tribology International* 2018; 124: 238-246, <https://doi.org/10.1016/j.triboint.2018.04.012>.
4. Bolewski Ł, Szkodo M, Kmiec M. Cavitation erosion degradation of Belzona® coatings. *Advances in Materials Science* 2017; 17(1): 22-33, <https://doi.org/10.1515/adms-2017-0002>.
5. Ciubotariu C R, Secosan E, Marginean G, Frunzaverde D, Campian V C. Experimental Study Regarding the Cavitation and Corrosion Resistance of Stellite 6 and Self-Fluxing Remelted Coatings. *Strojnicki Vestnik -Journal of Mechanical Engineering* 2016; 62 (3): 154-162, <https://doi.org/10.5545/sv-jme.2015.2663>.
6. Heathcock C J, Protheroe B E, Ball A. Cavitation erosion of stainless steels. *Wear* 1982; 81(2): 311-327, [https://doi.org/10.1016/0043-1648\(82\)90278-2](https://doi.org/10.1016/0043-1648(82)90278-2).
7. Kim J H, Lee M H. A Study on Cavitation Erosion and Corrosion Behavior of Al-, Zn-, Cu-, and Fe-Based Coatings Prepared by Arc Spraying. *Journal of Thermal Spray Technology* 2010; 19(6): 1224-1230, <https://doi.org/10.1007/s11666-010-9521-0>.
8. Krella A. Cavitation degradation model of hard thin PVD coatings. *Advances in Materials Science* 2010; 10(3): 27-36, <https://doi.org/10.2478/v10077-010-0010-4>.
9. Kumar H, Chittosiya C, Shukla V.N. HVOF Sprayed WC Based Cermet Coating for Mitigation of Cavitation, Erosion & Abrasion in Hydro Turbine Blade, *MATERIALS TODAY-PROCEEDINGS* 2018; 5(2): 6413-6420. <https://doi.org/10.1016/j.matpr.2017.12.253>
10. Krumenacker L, Fortes-Patella R, Archer A. Numerical estimation of cavitation intensity. *IOP Conference Series-Earth and Environmental Science* 2014; 22: Article Number: UNSP 052014, <https://doi.org/10.1088/1755-1315/22/5/052014>.
11. Kwok C T, Man H C, Cheng F T. Cavitation erosion and damage mechanisms of alloys with duplex structures. *Materials Science and Engineering A242* 1998: 108-120, [https://doi.org/10.1016/S0921-5093\(97\)00514-5](https://doi.org/10.1016/S0921-5093(97)00514-5).
12. Steller J, Krella A, Koronowicz J, Janicki W. Towards quantitative assessment of material resistance to cavitation erosion. *Wear* 2005; 258: 604-613, <https://doi.org/10.1016/j.wear.2004.02.015>.
13. Waliszyn A, Adamkiewicz A. A method of vibration damping for diesel engine cylinder lines to prevent the consequences of erosion. *Eksploracja i Niezawodność - Maintenance and Reliability* 2018; 20: 371-377, <https://doi.org/10.17531/ein.2018.3.4>.
14. Yang D, Yu A, Ji B, Zhou J, Luo X. Numerical analyses of ventilated cavitation over a 2-D NACA0015 hydrofoil using two turbulence modeling methods. *Journal of Hydrodynamics* 2018; 30(2): 345-356, <https://doi.org/10.1007/s42241-018-0032-7>.
15. Yu A, Luo X, Ji B. Analysis of ventilated cavitation around a cylinder vehicle with nature cavitation using a new simulation method. *Science Bulletin* 2015; 60(21): 1833-1839, <https://doi.org/10.1007/s11434-015-0916-7>.

Aleksandr WALISZYN
Andrzej ADAMKIEWICZ

Maritime University of Szczecin, Faculty of Marine Engineering
Wały Chrobrego 1-2, 70-500 Szczecin, Poland

E-mail: a.valishin@am.szczecin.pl, a.adamkiewicz@am.szczecin.pl